Title
Crystal structure of an idiotype-anti-idiotype Fab complex.

Journal
Proceedings of the National Academy of Sciences of the United States of America, 91(5)

ISSN
0027-8424

Authors
Ban, N
Escobar, C
Garcia, R
et al.

Publication Date
1994-03-01

DOI
10.1073/pnas.91.5.1604

Proc. Natl. Acad. Sci. USA
Vol. 91, pp. 1604–1608, March 1994
Immunology

Crystal structure of an idiotype–anti-idiotype Fab complex

(x-ray crystallography/protein structure/internal-image antibody)

NENAD BAN*, CARLOS ESCOBAR†, ROBYN GARCIA†, KARL HASEL†, JOHN DAY*, AARON GREENWOOD*, AND ALEXANDER MCPHERSON*‡

*Department of Biochemistry, University of California, Riverside, CA 92521; and †Immunopharmaceutics, Inc., 11011 Via Frontera, San Diego, CA 92127

Communicated by Joseph Kraut, November 15, 1993

ABSTRACT **Anti-idiotypic monoclonal antibody 409.5.3 is raised against an antibody that neutralizes feline infectious peritonitis virus. This antibody, used as an immunogen, elicits the production of anti-anti-idiotypic antibodies that in turn neutralize the virus. The crystal structure of the complex between anti-idiotypic Fab 409.5.3 and idiotypic Fab fragment of virus-neutralizing antibody has been solved by molecular replacement using real-space Patterson search and filtering by Patterson correlation-coefficient refinement. The structure has been refined to an *R* value of 0.21 based on 21,310 unique reflections between 40.0 and 2.9 Å. The three-dimensional structure reveals extensive, specific interactions that involve 118 van der Waals contacts and at least 9 probable hydrogen bonds. The two Fabs are rotated 61° with respect to each other around the approximate long axis of the complex and are within 26° of being aligned along their major axes.**

According to the Jerne hypothesis (1), the immune system responds to foreign substances as a regulatory network composed of idiotypes (Ab1s) and their anti-idiotypes (Ab2s) (for reviews see refs. 2 and 3). The antibody Ab1 made in response to the original antigen becomes itself an antigen and elicits the synthesis of a secondary antibody, or Ab2. This response can be divided into an antigen-noninhibitable group (Ab2α) and an antigen-inhibitable group (Ab2β). A third group, which is antigen-inhibitable because of steric hindrance with the antigen binding site, is designated Ab2γ (reviewed in ref. 4). Idiotypes are the sum of idiotopes or serologically determined antigenic determinants unique to an antibody or group of antibodies. Ab2s produced against the combining-site idiotope may carry an "internal image" of the external antigen and are also known as internal-image antibodies. A true internal-image molecule can induce immune-mediated responses similar to those induced by the original antigen, and this property has, in fact, been used to produce vaccines (reviewed in refs. 5 and 6). Thus, there may be significant structural mimicry between the complementarity-determining regions (CDRs) of internal-image Ab2s and the original antigen. However, such accurate molecular mimicry was not observed when the interaction between lysozyme and an anti-lysozyme antibody (D1.3) was compared with the interaction between D1.3 and the anti-idiotope (E225) (7).

For the idiotope–anti-idiotope complex structure described here,§ the original antigen was the E2 peplomer, a large glycoprotein, of feline infectious peritonitis virus (FIPV). The E2 peplomer was chosen as an antigen because it is responsible for: (*i*) binding of virus to plasma membranes of susceptible cells, (*ii*) cell fusion, (*iii*) induction of cell-mediated cytotoxicity of infected cells, and (*iv*) induction of neutralizing antibody (8). This virus produces a fatal disease in both wild and domestic cats that has defied conventional vaccines (9). A salient observation was that Ab2 409.5.3, when injected back into mice, elicited the production of Ab3s that had FIPV neutralizing properties. This indicated that the combining properties of the original epitope were transmitted by the Ab2 (C.E., E. Skaletsky, J. Anderson, A. Rudin, K. Frericks, and K.H., unpublished data).

MATERIALS AND METHODS

Preparation of Crystals. Isolation and characterization of the mouse monoclonal IgG2a Ab1 730.1.4 and the corresponding IgG1 Ab2 409.5.3 have been described (9). The complex was crystallized by vapor diffusion from solutions containing 45% saturated ammonium sulfate and 7 mg of protein per ml at pH 7.0 and 23°C (10). Silver staining of redissolved crystals after SDS/PAGE under nonreducing conditions demonstrated the crystals to contain both Fab fragments and in equal amounts. Crystals were of space group $P2_122_1$ with unit cell dimensions a = 75.2 Å, b = 80.6 Å, and c = 187.6 Å (1 Å = 0.1 nm). Assuming two Fab molecules in the asymmetric unit, we calculated the solvent content of the crystal as 57% (V_m = 2.84 Å^3/D) (11).

Diffraction Data. Five crystals were used to collect x-ray diffraction data at 18°C with a two-detector Xuong–Hamlin (12) multiwire area detector system. The data were processed with the programs of Howard and Nielson and coworkers (13). The crystals, although small, diffract x-rays to 2.9 Å but decay rapidly in the x-ray beam. In all, 89,898 observations were measured and reduced to 23,640 unique reflections with R_{sym} = 0.112. This represents 92% of theoretically observable reflections to 2.9-Å resolution. Structure refinement included data of $F > 3\sigma$ (21,310 unique reflections; 83% complete from 40 to 2.9 Å; 47% between 3.1 and 2.9 Å).

Molecular Replacement. The structure was solved by use of molecular replacement and Patterson correlation-coefficient (PC) refinement with version 3.1 of the program X-PLOR (14) running on an SGI 320 VGX or the San Diego Cray-YMP computers. The real-space Patterson search method of Huber (15) was used for the cross rotation of five model Fab molecules (R19.9, McPC603, KOL, J539, and HyHel-5; refs. 16–20) from the Protein Data Bank (21) (entries 2F19, 1MCP, 2FB4, 2FBJ, and 2HFL) against the idiotope–anti-idiotope data. Translation searches used the method of Fujinaga and Read (22) and were carried out with X-PLOR on 15- to 4-Å data and 1-Å sampling interval.

Abbreviations: Ab1, idiotypic antibody; Ab2, anti-idiotypic antibody; Ab3, anti-anti-idiotypic antibody; Ab2β, internal-image antibody; PC, Patterson correlation coefficient; CDR, complementarity-determining region; FIPV, feline infectious peritonitis virus.

‡To whom reprint requests should be addressed.

§The atomic coordinates have been deposited in the Protein Data Bank, Chemistry Department, Brookhaven National Laboratory, Upton, NY 11973 (reference 1IAI). This information is embargoed for 2 years from the date of publication.

The publication costs of this article were defrayed in part by page charge payment. This article must therefore be hereby marked "*advertisement*" in accordance with 18 U.S.C. §1734 solely to indicate this fact.

Atomic Refinement. Rigid-body refinement, Powell minimization (23), simulated annealing (24), and *B*-factor refinement employed X-PLOR (14). An atomic model was fitted to both $2F_o - F_c$ and $F_o - F_c$ electron density maps by using FRODO (25) and O (26). Omit maps were calculated after removal of 40-residue segments of the model (5% of the asymmetric unit) followed by 50 cycles of Powell minimization using data between 40- and 2.9-Å resolution and employing a bulk solvent mask calculated by X-PLOR.

Structure Analysis. Buried area of the molecule was calculated with MS (27) using a probe radius of 1.7 Å. Pairwise interactions were calculated with S. Sheriff's program CONTACSYM using standard van der Waals radii (28). ATMSRF (S. Sheriff) was used to calculate the surface area by residue. SUMCONT and SUMAREA (S. Sheriff) were used to attribute interactions and surface areas to various parts of the molecule. Unless otherwise indicated, the amino acid numbering scheme used here for both Fabs follows the convention of Kabat *et al.* (29).

RESULTS AND DISCUSSION

Structure Determination. Cross-rotational searches were carried out with X-PLOR using individual constant (C) and variable (V) domains as well as 12 models for each complete Fab molecule, each constructed with elbow angles varying from 125° to 180° in increments of 5°. Assuming the correct orientation to be among the maxima of the rotation function, we filtered the search results by PC refinement (30, 31). Cross-rotation searches performed with MERLOT (32) were inconclusive. PC refinement consisted of 15 steps of conjugate gradient minimization using the method of Powell (23) for the orientation of the whole molecule, followed by 40 increments of orientational and translational refinement of the C and V domains using 12.0- to 4.0-Å data. The highest correlation coefficient obtained was only 0.068. Rotational and translational parameters of solutions yielding the 10 highest correlation coefficients were then further refined by treating the heavy- and light-chain V (V_H and V_L) domains, the first heavy-chain C (C_H1) domain, and the light-chain C (C_L) domain as rigid bodies.

Two orientations, A and B, that yielded relatively high correlation coefficients were chosen for further analysis. All models were rotated according to these solutions and subjected to PC refinement. Models McPC603 (17) and HyHel-5 (20), both with elbow angles altered to 140°, yielded the highest correlation coefficients (0.085 and 0.078 with signal/noise ratios of 1.4 and 1.18, respectively). Translations between molecules A and B in the asymmetric unit were determined by applying the translation according to the PC in a triclinic unit cell having the real unit cell parameters (correlation coefficient, 0.132; signal/noise, 1.28).

A model containing both Fabs was used in translation function searches to establish the relative position of pairs of molecules related by twofold or screw axes (correlation coefficient, 0.248; signal/noise, 1.42). Rigid-body refinement of properly oriented and positioned molecules in the unit cell produced an *R* factor of 0.40 and correlation coefficient of 0.50 for reflections between 12.0 and 4.0 Å. Inspection of the packing demonstrated that there were no unacceptable contacts. As sequence information became available, models for both Fabs were constructed based on the sequence and conformations of canonical loops.

From the molecular replacement solution it was not obvious which of the Fab molecules in the asymmetric unit represented Fab1 (Fab of Ab1 730.1.4) and which was Fab2 (Fab of Ab2 409.5.3) though there is only 72% sequence identity. Subsequent refinement by simulated annealing and assumption of each possibility in turn, however, allowed discrimination. Both choices yielded *R* values of about 0.23, but one model maintained nearly ideal geometry for both Fab fragments. The other exhibited twice the deviations from ideal values for bond lengths and angles. Furthermore, in the case characterized by poor geometry, the free *R* factor (33) remained virtually unchanged during refinement, whereas the free *R* factor for the correct solution was reduced significantly.

Quality of $2F_o - F_c$ maps was good with the exception of exposed loops on C domains, which sometimes exhibited poorly ordered density. Omit maps confirmed the assignment of Fabs with the heavy-chain third (H3) hypervariable loops being, perhaps, most distinctive. This CDR in Fab1 and Fab2 has significantly different sequence and length. Hypervariable loops on V domains were stabilized by interactions and were clearly visible in electron density maps.

Nine cycles of model building were followed by simulated annealing (starting temperature, 3000 K) and then 120 cycles of conjugate gradient minimization. A temperature (*B*) factor of 15 Å^2 was maintained for all atoms. Four more cycles of rebuilding were carried out, followed by Powell minimization and restrained *B*-factor refinement where the target value for the deviations of *B* factors for bonded atoms was set to 1.5 Å^2 and that for bonded atoms related by bonded angles to 2.0 Å^2 (14). The average isotropic displacement parameter for all protein atoms is currently 7.3 Å^2. This value appears low but agrees with that from a Wilson plot (34) of 13 Å^2. The present *R* value for the complex structure with a bulk solvent correction is 0.21 for 21,310 reflections between 40.0 and 2.9 Å ($F > 3\sigma$). The rms deviations from ideal values for the following parameters are as follows: bond lengths, 0.015 Å; bond angles, 2.14°; dihedral angles, 28.8°; improper angles, 1.9°. No solvent molecules have been added to the model.

Description of Fabs. Both Fabs have similar elbow angles (138.2° for Fab1 and 141.4° for Fab2) consistent with values found for other Fabs (35, 36). Five hypervariable regions of Fab1 can be classified as $L1_2$, $L2_1$, $L3_1$, $H1_1$, and $H2_2$ (37). Loop H3 has 12 amino acids and forms a long hairpin structure that extends toward L2 and L1 on the light-chain domain. Two ridges on the surface of the combining site are formed by L1, L3, and H3 on one side and H1 and H2 on the other. Four hypervariable regions of Fab2 can be classified as belonging to the canonical structures $L2_1$, $L3_1$, $H1_1$, and $H2_4$ (37). Even though loop H1 can be classified as $H1_1$, it has a conformation different from the canonical structure: the side chain of Phe-27, instead of Phe-29 as in the canonical structure, is buried within the framework structure. On the other hand, Phe-29 of this loop is oriented toward the V_L–V_H domain interface and partially buried. Sequence analysis of Fab2 indicates that the L1 region belongs to the mouse κ light-chain subgroup IV (29). This loop has 10 residues, and main-chain atoms of residues 25–27a and 33 (canonical structure numbering) follow the canonical structure model. Hydrophilic serines between residues 29 and 31 form a turn that is one residue longer than the turn in loop $L1_1$ of HyHel-5. Loop H3 of Fab2 has 10 amino acids and forms a broad turn stabilized by a hydrogen bond between the side chain of Arg-94 and the carbonyl oxygen of Phe-97. The Fab2 CDR's surface is undulating with no deep grooves as are observed when the antigen is a small molecule (38). A shallow cavity exists between the L1, H3, and H2 loops.

Description of the Structure. Two views of the complex are shown in Fig. 1. The two Fabs interact by direct juxtaposition of their complementary CDRs. The Fabs are rotated by 61° about the long axis of the complex with respect to one another. The pseudo twofold axes relating V_L and V_H domains of the two fragments are nearly colinear, the angle between their axes being 154°. By this rotation, the heavy chain of one molecule is interacting almost entirely with the heavy chain of the other, and similarly light chain with light, but to a much lesser extent. The major axis of the complex

is ≈140 Å and it is oriented along the 187.6-Å *c* axis of the unit cell (Fig. 2).

Idiotope–Anti-Idiotope Interface. Surface representations of the CDRs that form the interface between the two Fabs are shown in Fig. 3. There is a striking degree of structural and chemical complementarity between the two, consistent with observations for other antibody–antigen complexes (38). Even though water molecules cannot be reliably visualized at 2.9-Å resolution, there appear to be no buried waters in the interface. Upon complex formation 1750 Å^2 are buried. Of this surface, Fab1 accounts for 860 Å^2 and Fab2 for 890 Å^2. These values are significantly greater than the values observed with Fab–lysozyme complexes but close to the buried surface area in the case of a Fab–neuraminidase complex, which conceals about 885 Å^2 for the Fab and 878 Å^2 for the neuraminidase (40). The heavy chain of 409.5.3 dominates the

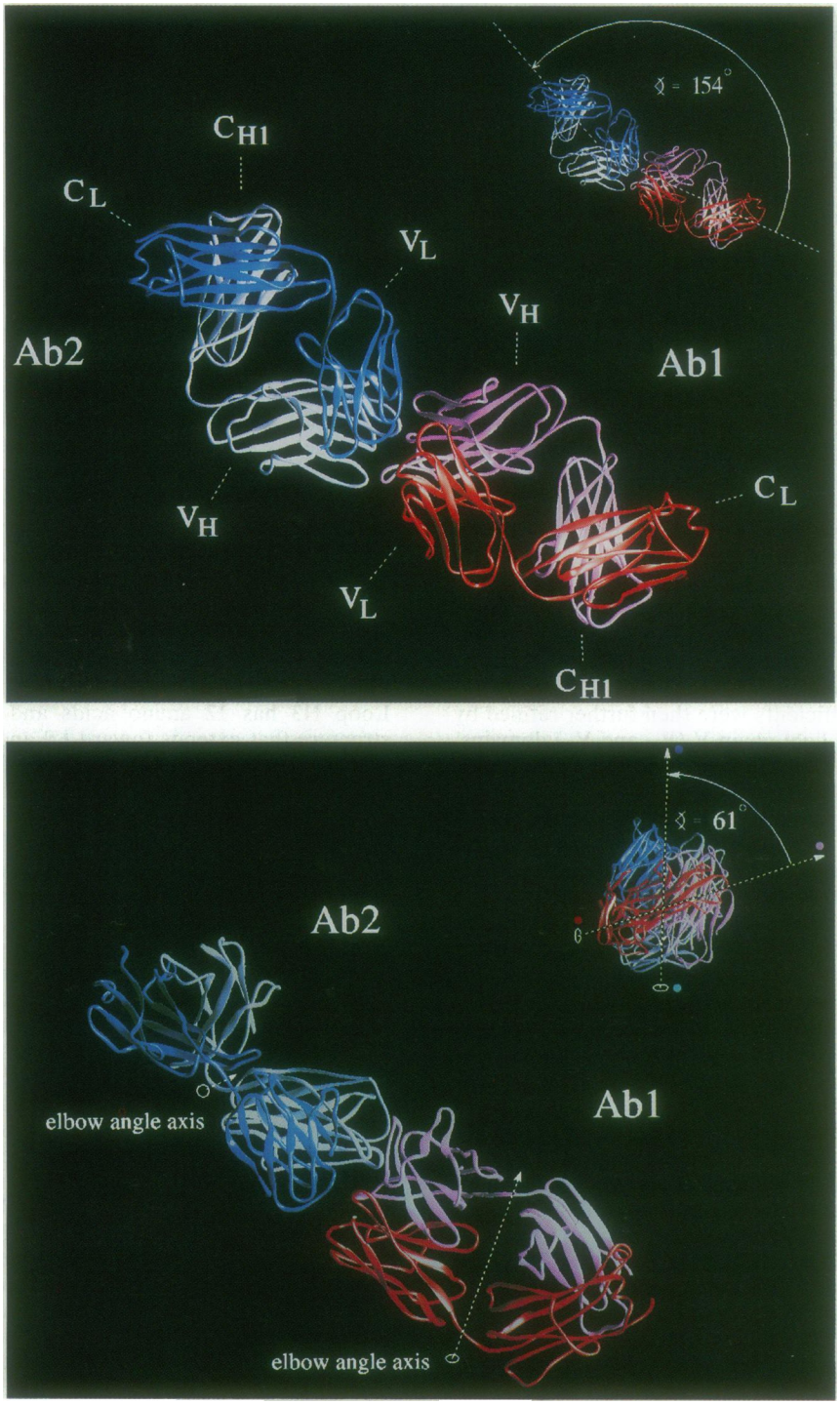

FIG. 1. (*Upper*) Structure of the Fab1–Fab2 complex. Anti-idiotypic Fab (labeled Ab2) is in light (heavy chain) and dark (light chain) blue. Idiotypic Fab (labeled Ab1) is in pink (heavy chain) and red (light chain). The pseudo twofold axis relating V_L and V_H domains of one Fab forms a 154° angle with the axis relating equivalent domains of the other Fab. This is schematically represented in the *Inset*. (*Lower*) A second view of the complex. Elbow angle axis vectors are indicated on Fab1 and Fab2. Relative rotation of two Fabs with respect to each other around the approximate long axis of the complex is 61°, as shown in the *Inset*. This angle was calculated by projecting two elbow angle axes onto the plane perpendicular to the long axis of the molecule. Axes for each Fab were established by the coordinates of two C^α atoms at the center of switch peptides. The figure was generated with RIBBONS (39).

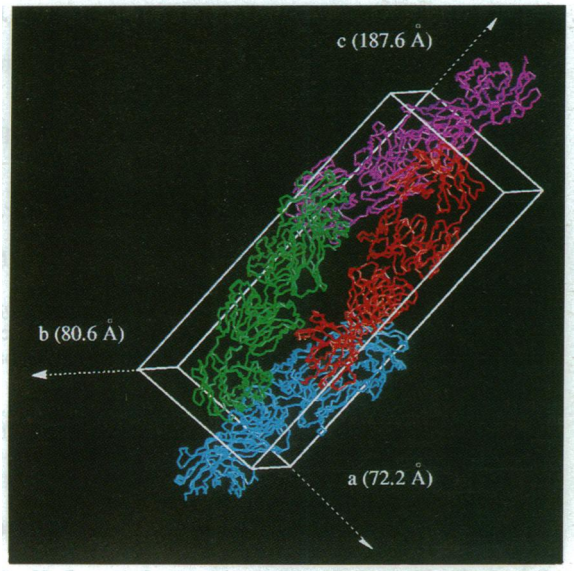

FIG. 2. Packing of the idiotope–anti-idiotope complex in the orthorhombic $P2_122_1$ unit cell viewed approximately down the crystallographic *b* axis. Directions of twofold and pseudo twofold axes are indicated by arrows. Four symmetry-related molecules are shown in different colors. The figure was generated from a cylinder file by RIBBONS (39).

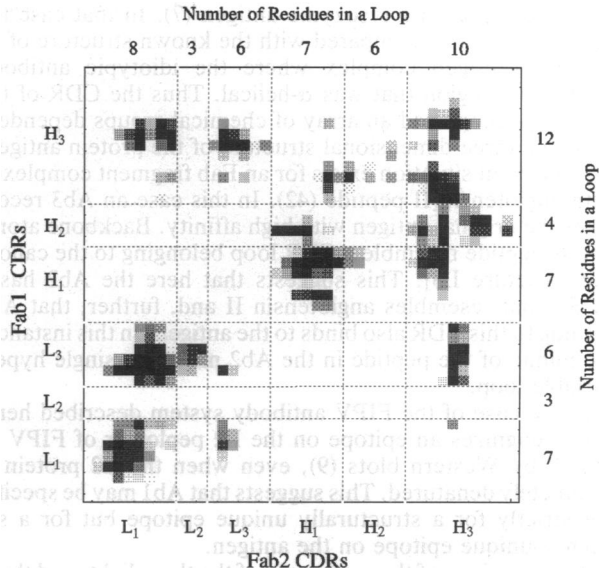

FIG. 4. Distance matrix between Fab1 and Fab2 CDRs. Specific loops for each Fab and the corresponding number of residues are indicated. Sizes of hypervariable regions are according to the structural classification of Chothia (37) except for loops H3, which follow the convention of Kabat (29). Density of the square in the matrix is a function of distance, ranging from darkest < 6.5 Å to lightest at 12.5 Å. Distances were calculated with X-PLOR between mass-weighted centroids of residues.

binding and contributes 63% of the surface area of the anti-idiotope buried in the complex. The surface of the Fab1 CDR is slightly concave so that Fab2, the antibody in this system, protrudes into it.

Hypervariable loops of two Fabs in contact through van der Waals interactions and hydrogen bonds are L1 (minor contributor), L3, H1, H2, and H3 of Fab1 (58 atoms) and L1, L3 (minor contributor), H1, H2, and H3 of Fab2 (59 atoms). Loops L1, L2, H1, and H2 on one Fab are in proximity to loops L1, L3, H1, and H3, respectively, on the other molecule (Fig. 4). In total, 19 residues of the idiotope and 17 residues of the anti-idiotope participate in 111 long van der Waals interactions < 4.11 Å and 7 short interactions < 3.44 Å (41). The complex is further stabilized by nine hydrogen bonds where the maximum distance between electronegative atoms is 3.5 Å.

The 730.1.4 idiotope is predominately located on its heavy chain, which contributes 71% to the buried area on the idiotope. Since V_H domains usually contribute more surface area in antibody–protein interactions (38), it is likely that this domain dominates the interaction between the idiotypic antibody and the antigen. In the structure of another idiotope–anti-idiotope complex (anti-lysozyme D1.3 Fab and its anti-idiotypic E225 Fab) (7), both Fabs are centered on V_L domains of opposing Fabs and interact primarily through their V_L domains. On the other hand, the V_H domain of idiotypic Fab D1.3 dominates the interaction with lysozyme. This is why the paratope and idiotope in the D1.3–E225 system overlap only partially, thus reducing the potential for total molecular mimicry.

Anti-Idiotypic Mimicry. Even though internal image idiotopes are three-dimensional amino acid constructs they can mimic protein, carbohydrate, or lipid epitopes. The structure of the D1.3–E225 complex involved an antibody against a

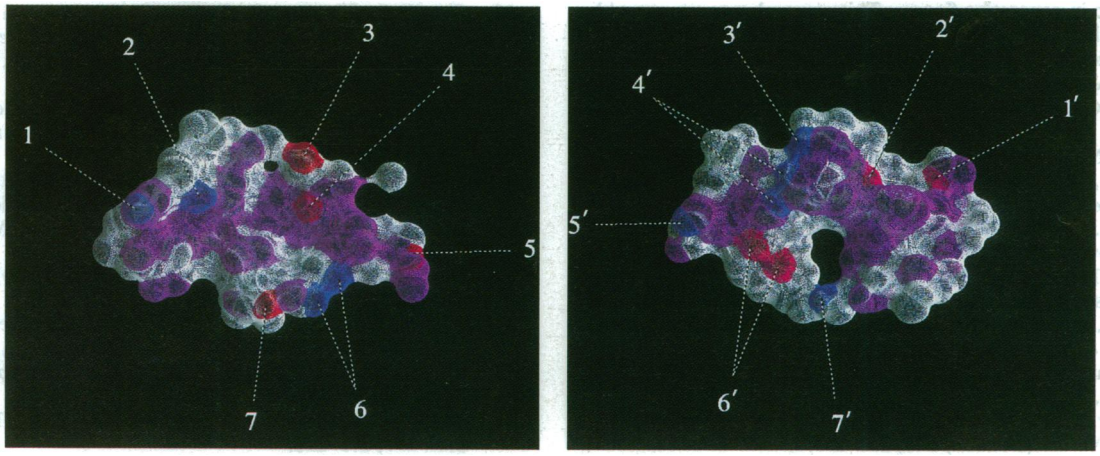

FIG. 3. Accessible surface area of the interacting region on the Fab1 idiotope is shown (*Left*) along with that of the Fab2 anti-idiotope (*Right*). This region is buried upon complex formation. Surfaces of atoms involved in van der Waals contacts are colored purple. Hydrogen bond donors are displayed in blue and hydrogen bond acceptors are in red. Eight groups involved in hydrogen bonding are labeled to facilitate identification of contact points between Fab1 and Fab2. The atoms on the idiotope are labeled clockwise with numbers 1–7 and those on the anti-idiotope counterclockwise with numbers 1′–7′. The surface was calculated by the MS option of RIBBONS (39) with a 1.7-Å probe.

known epitope on a lysozyme antigen (7). In that case the complex could be compared with the known structure of an antibody–antigen complex where the idiotypic antibody bound to a region that was α-helical. Thus the CDR of the antibody recognized an array of chemical groups dependent upon the three-dimensional structure of the protein antigen.

A different situation exists for an Fab fragment complexed with angiotensin II peptide (42). In this case an Ab3 recognizes the original antigen with high affinity. Backbone atoms of this peptide resemble a CDR loop belonging to the canonical structure $L3_1$. This suggests that here the Ab2 has a CDR3 that resembles angiotensin II and, further, that Ab3 binding to this CDR also binds to the antigen. In this instance, the mimic of the peptide in the Ab2 may be a single hypervariable loop.

In the case of the FIPV antibody system described here, Ab1 recognizes an epitope on the E2 peplomer of FIPV as shown by Western blots (9), even when the E2 protein is completely denatured. This suggests that Ab1 may be specific not strictly for a structurally unique epitope but for a sequence-unique epitope on the antigen.

A comparison of the sequences of the three light- and three heavy-chain CDRs with the known sequence of the antigen shows homology in two instances. In both L1 and H1 there is near identity with sequences of six residues that occur in the antigen. The L1 CDR sequence is Val-Ser-Ser-Ser-Ile-Ser, which differs with the segment on the E2 peplomer beginning at position 276 having sequence Ile-Ser-Ser-Ser-Ile-Ser by the conservative substitution of valine for isoleucine at the first position. Similarly, the H1 loop is Gly-Phe-Thr-Phe-Asn-Asn, which matches the Gly-Phe-Ser-Phe-Asn-Asn sequence of the antigen beginning at residue 1451. Here again, only a conservative change, serine to threonine, marks a difference. These two regions of homology on the anti-idiotope provide important contacts with the Ab1 originally produced in response to antigen. Homologous residues on L1 of the anti-idiotope are involved in 36 van der Waals contacts and 2 hydrogen bonds, and those on H1 form 18 van der Waals contacts and 1 hydrogen bond. The possibility exists, therefore, that antigen sequence information determining specificity may in fact be preserved through the Ab1 and be made to reappear in the structure of the Ab2 response.

We thank Tzu-Ping Ko and Steven B. Larson for advice and discussions and Steven Sheriff for programs used to analyze interactions between molecules. We thank the San Diego Supercomputer Facility for time on the Cray Y-MP and the Academic Computing Graphics and Visual Imaging Lab, University of California, Riverside, for help in generating figures. This research was supported by grants from the National Institutes of Health (GM40706-03), from the National Science Foundation, and from the National Aeronautics and Space Administration (NAG8-804), as well as by the Immunopharmaceutics Corporation of San Diego.

1. Jerne, N. K. (1974) *Ann. Immunol. Paris* **125C**, 373–389.
2. Greene, M. I. & Nisonoff, A., eds. (1984) in *The Biology of Idiotypes* (Plenum, New York).
3. Davie, J. M., Seiden, M. V., Greenspan, N. S., Lutz, C. T., Bartolow, T. L. & Clevinger, B. L. (1986) *Annu. Rev. Immunol.* **4**, 147–165.
4. Dalgleish, A. G. & Kennedy, R. C. (1988) *Vaccine* **6**, 215–220.
5. Poskitt, D. C., Jean-Francois, M. J. B., Turnbull, S., MacDonald, L. & Yasmeen, D. (1991) *Vaccine* **9**, 792–796.
6. Williams, W. V., Weiner, D. B., Kieber-Emmons, T. & Greene, M. I. (1990) *Trends Biotechnol.* **8**, 256–263.
7. Bentley, G. A., Boulot, G., Riottot, M. M. & Poljak, R. J. (1990) *Nature (London)* **348**, 254–257.
8. Sturman, L. S. & Holmes, K. V. (1983) *Adv. Virus Res.* **28**, 35–112.
9. Escobar, J. C., Kochik, S. A., Skaletsky, E., Rosenberg, J. S. & Beardsley, T. R. (1992) *Viral Immun.* **1**, 71–79.
10. Ban, N., Carlos, J. C., Day, J., Greenwood, A. & McPherson, A. (1993) *J. Mol. Biol.* **234**, 894–896.
11. Matthews, B. W. (1968) *J. Mol. Biol.* **33**, 491–497.
12. Xuong, N.-H., Nielson, C., Hamlin, R. & Anderson, D. (1985) *J. Appl. Crystallogr.* **18**, 342–360.
13. Hamlin, R., Cork, C., Howard, A., Nielson, C., Vernon, W., Mathews, D. & Xuong, N.-H. (1981) *J. Appl. Crystallogr.* **14**, 85–89.
14. Brünger, A. T. (1993) *X-PLOR Manual* (Yale University, New Haven, CT), Version 3.1.
15. Huber, R. (1985) in *Molecular Replacement: Proceedings of the Daresbury Study Weekend, Daresbury, February, 1985*, compiled by P. A. Mechin (Science and Engineering Research Council, Daresbury, U.K.), pp. 58–61.
16. Lascombe, M.-B., Alzari, P. M., Boulot, G., Saludjian, P., Tougard, P., Bareh, C., Haba, S., Rosen, E. M., Nisonoff, A. & Poljak, R. J. (1989) *Proc. Natl. Acad. Sci. USA* **86**, 607–611.
17. Satow, Y., Cohen, G. H., Padlan, E. A. & Davies, D. R. (1986) *J. Mol. Biol.* **190**, 593–604.
18. Marquart, M., Deisenhofer, J., Huber, R. & Palm, W. (1980) *J. Mol. Biol.* **141**, 369–391.
19. Suh, S. W., Bhat, T. N., Navia, M. N., Cohen, G. H., Rao, D. N., Rudikoff, S. & Davies, D. R. (1986) *Proteins Struct. Funct. Genet.* **1**, 74–80.
20. Sheriff, S., Silverton, E. W., Padlan, E. A., Cohen, G. H., Smith-Gill, S. J., Finzel, B. C. & Davies, D. R. (1987) *Proc. Natl. Acad. Sci. USA* **84**, 8075–8079.
21. Bernstein, F. C., Koetzle, T. F., Williams, G. J. B., Meyer, E. F., Jr., Brice, M. D., Rodgers, J. R., Kennard, O., Shimanouchi, T. & Tasumi, M. (1977) *J. Mol. Biol.* **112**, 535–542.
22. Fujinaga, M. & Read, R. J. (1987) *J. Appl. Crystallogr.* **20**, 517–521.
23. Powell, M. J. D. (1977) *Math. Prog.* **12**, 241–254.
24. Brünger, A. T., Kuriyan, J. & Karplus, M. (1987) *Science* **235**, 458–460.
25. Jones, T. A. (1978) *J. Appl. Crystallogr.* **11**, 268–272.
26. Jones, T. A. & Kjeldgaard, M. (1990) *"O" Manual* (Uppsala University, Sweden and Aarhus University, Denmark), Version 5.4.
27. Connolly, M. L. (1983) *J. Appl. Crystallogr.* **16**, 548–558.
28. Gelin, B. R. & Karplus, M. (1979) *Biochemistry* **8**, 1256–1268.
29. Kabat, E. A., Wu, T. T., Perry, H. M., Gottesman, K. S. & Foeller, C. (1991) *Sequences of Proteins of Immunological Interest* (Public Health Service, National Institutes of Health, Washington, DC), 5th Ed.
30. Hauptman, H. (1982) *Acta Crystallogr. Sect. A* **38**, 289–294.
31. Brünger, A. T. (1990) *Acta Crystallogr. Sect. A* **46**, 46–57.
32. Fitzgerald, P. M. D. (1988) *J. Appl. Crystallogr.* **21**, 273–278.
33. Brünger, A. T. (1992) *Nature (London)* **355**, 472–475.
34. Wilson, A. J. C. (1949) *Acta Crystallogr.* **2**, 318–321.
35. Sheriff, S., Silverton, E., Padlan, E. A., Cohen, G., Smith-Gill, S., Finzel, B. & Davies, D. R. (1988) in *Structure and Expression*, eds. Sarma, M. & Sarma, R. H. (Adenine, New York), Vol. 1, pp. 49–54.
36. Padlan, E. A., Silverton, E. W., Sheriff, S., Cohen, G. H., Smith-Gill, S. J. & Davies, D. R. (1989) *Proc. Natl. Acad. Sci. USA* **86**, 5938–5942.
37. Chothia, C., Lesk, A. M., Tramontano, A., Levitt, M., Smith-Gill, S. J., Air, G., Sheriff, S., Padlan, E. A., Davies, D., Tulip, W. R., Colman, P. M., Spinelli, S., Alzari, P. M. & Poljak, R. J. (1989) *Nature (London)* **342**, 877–883.
38. Davies, D. R., Padlan, A. E. & Sheriff, S. (1990) *Annu. Rev. Biochem.* **59**, 439–473.
39. Carson, M. & Bugg, C. E. (1986) *J. Mol. Graphics* **4**, 121–122.
40. Tulip, W. R., Varghese, J. N., Webster, R. G., Air, G. M., Laver, W. G. & Colman, P. M. (1989) *Cold Spring Harbor Symp. Quant. Biol.* **54**, 257–263.
41. Sheriff, S., Hendrickson, W. A. & Smith, J. L. (1987) *J. Mol. Biol.* **197**, 273–296.
42. Garcia, K. C., Ronco, P. M., Verroust, P. J., Brünger, A. T. & Amzel, L. M. (1992) *Science* **257**, 502–507.